Generating macroscopic superposition states in nanomechanical graphene resonators

A. Voje, J. M. Kinaret, and A. Isacsson*

Department of Applied Physics, Chalmers University of Technology, SE-412 96 Göteborg, Sweden

(Received 24 November 2011; revised manuscript received 27 April 2012; published 10 May 2012)

A theoretical study of the quantum dynamics of a symmetric nanomechanical graphene resonator with degenerate flexural modes is presented. Applying voltage pulses to two back gates, flexural vibrations of the membrane can be selectively actuated and manipulated. For graphene, nonlinear response becomes important for amplitudes comparable to the magnitude of zero-point fluctuations. We show, using analytical and numerical methods, that this allows for creation of catlike superpositions of coherent states as well as superpositions of coherent catlike nonproduct states.

DOI: 10.1103/PhysRevB.85.205415 PACS number(s): 85.85.+j, 42.50.Dv, 73.50.Fq

Coherent superposition of states are characteristic traits of quantum mechanics. These phenomena have already been realized in many-particle contexts such as trapped ultracold atoms,[1] superconductors,[2] and photonic systems.[3] A current challenge is to observe these effects for collective degrees of freedom in a macroscopic context in, e.g., mechanical resonators.[4]

Recent advances in cooling mechanical resonators and sensitive displacement detection have allowed reaching the motional ground state and observing zero point fluctuations of center of mass.[5,6] Active manipulation and characterization of the quantum state of these systems, as already achieved with photons,[7] seem to be within reach. For a mechanical system, a desirable state to generate is a "cat" state. This is a coherent superposition of two minimum uncertainty wave packets separated by more than their individual quantum fluctuations.

For the harmonic oscillator, a minimum uncertainty wave packet is a coherent state $|\alpha\rangle = \exp[\alpha a^\dagger - \alpha^* a]|0\rangle$ generated by displacing the oscillator ground state.[8] As shown by Yurke and Stoler,[9] for a nonlinear oscillator $H = \hbar\omega_0\hat{n} + \hbar\Omega\hat{n}^2$, an initial coherent state $|\alpha\rangle$ will after a time $t = \pi/(2\Omega)$ evolve into the cat state $(1/\sqrt{2})[e^{-i\pi/4}|\alpha\rangle + e^{i\pi/4}|-\alpha\rangle]$ with the maximum spatial separation $\Delta = 2|\alpha|$.

Nanoelectromechanical resonators are typically intrinsically nonlinear.[10] Recent theoretical studies of their quantum dynamics show that it differs from the classical motion[11,12] and the nonlinearity can be exploited in the detection of the quantum signatures. The amplitudes needed to observe nonlinear effects are often orders of magnitude larger than the quantum zero-point fluctuations $x_0 = \sqrt{\hbar/m\omega_0}$. A cat state obtained due to this nonlinearity would have a separation $\Delta \gg 1$. As the decoherence rate scales as Δ^2 (see Refs. 13 and 14), this has, until now, been unfeasible. Instead, coupling to auxiliary quantum systems has been proposed to engineer the nonlinearity.[15,16]

We show how, in the limit $k_B T \ll \hbar\omega_0$, the intrinsic nonlinearity of a graphene membrane resonator can be used to prepare cat states by applying voltage pulses to local backgates. The reason for using graphene is the ultralow mass of the graphene sheet, which leads to a large x_0, and an onset of nonlinear response at small amplitudes.[17,18] This implies that cat states with moderate Δ can be constructed without the need for engineered auxiliary quantum systems or feedback loops. Another feature of two-dimensional mechanical resonators is that they can be designed to have degenerate flexural modes. Coupling between these modes can be externally controlled using, e.g., gate electrodes, which can be utilized for state manipulation.

For concreteness we consider a square graphene membrane with mass density $\rho_0 = 7.6 \times 10^{-7}$ kg/m^2 and side length L. The sheet is suspended in the xy plane at a distance u_0 above two local backgates (see Fig. 1). They cover adjacent quadrants below the membrane and have voltages $V_1(t)$ and $V_2(t)$. The Hamiltonian density of the system can be divided into two parts: $\mathscr{H} = \mathscr{H}_0(\mathbf{x}) + \mathscr{H}_G(\mathbf{x}, V_1, V_2)$, where $\mathbf{x} \equiv (x, y)$. Here $\mathscr{H}_0(\mathbf{x})$ gives the intrinsic mechanics of the membrane while the coupling to the gates is described in $\mathscr{H}_G(\mathbf{x}, V_1, V_2)$. To a first approximation one finds[17,19]

$$\mathscr{H}_0 = \frac{\pi_0^2}{2\rho_0} + \frac{T_0}{2}|\nabla u|^2 + \frac{T_1}{4}|\nabla u|^4, \tag{1}$$

where $u(\mathbf{x},t)$ is the out-of-plane displacement and π_0 its conjugate momentum density. The built-in tension is T_0 and the stretching-induced tension is determined by $T_1 = (\mu + \lambda/2)$, where the Lamé-parameters of graphene are $\mu \approx 3\lambda \approx 9$ eV/Å^2.[20] The bending term $\kappa_g|\nabla^2 u|^2/2$, where κ_g is the graphene bending rigidity of $\kappa_g \approx 1$ eV, is much smaller than the stretching term, and is therefore omitted from Eq. (1). We model $\mathscr{H}_G$ in the local approximation as $\mathscr{H}_G = \epsilon_0 V(\mathbf{x},t)^2/2[u_0 + u(\mathbf{x})]$, where $\epsilon_0 = 8.854 \times 10^{-12}$ F/m and $V(\mathbf{x},t)$ is the local gate potential. Expanding u and π_0 in mode functions as

$$u = \sum_{\mathbf{k}} q_{\mathbf{k}}(t)\varphi_{\mathbf{k}}(\mathbf{x}), \quad \pi_0 = \frac{1}{L^2}\sum_{\mathbf{k}} p_{\mathbf{k}}(t)\varphi_{\mathbf{k}}(\mathbf{x}), \tag{2}$$

and using $\varphi_{\mathbf{k}} = 2\sin(k_x x)\sin(k_y y)$ and $\mathbf{k} = (k_x, k_y) = (n,m)\pi/L$ for $n,m = 1,2,\ldots$, gives $H = H_0 + H_G$ with

$$\begin{aligned} H_0 &= \sum_{\mathbf{k}} \frac{1}{2M}\left(p_{\mathbf{k}}^2 + M^2\omega_{\mathbf{k}}^2 q_{\mathbf{k}}^2\right) \\ &\quad + \frac{1}{2}\sum_{\mathbf{k}\mathbf{k}'}\sum_{\mathbf{k}''\mathbf{k}'''} F_{\mathbf{k}\mathbf{k}'\mathbf{k}''\mathbf{k}'''}(q_{\mathbf{k}} q_{\mathbf{k}'} q_{\mathbf{k}''} q_{\mathbf{k}'''}), \\ H_G &= K_0 + \sum_{\mathbf{k}} K_{\mathbf{k}} q_{\mathbf{k}} + \frac{1}{2}\sum_{\mathbf{k}\mathbf{k}'} K_{\mathbf{k}\mathbf{k}'} q_{\mathbf{k}} q_{\mathbf{k}'}. \end{aligned} \tag{3}$$

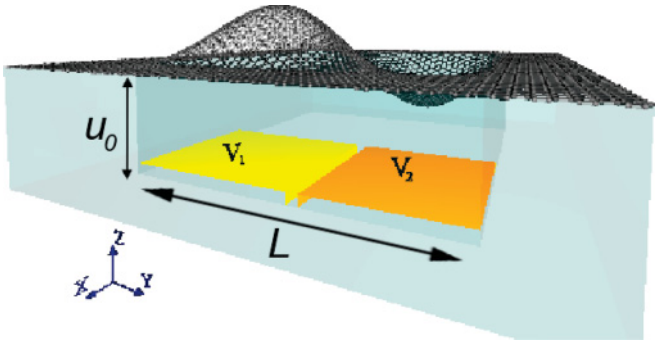

FIG. 1. (Color online) Cross section of a square graphene membrane resonator. A fully clamped graphene membrane with side L is suspended a distance u_0 above the substrate. Below, covering two adjacent quadrants beneath the membrane, are local backgates with time-dependent voltage biases $V_{1,2}(t)$. By applying pulses to the local gates, catlike superpositions of flexural mode states, as well as superpositions of coherent catlike nonproduct states, can be generated.

Here $M = \rho_0 L^2$ and $\omega_{\mathbf{k}} = (T_0/\rho_0)^{\frac{1}{2}}|\mathbf{k}|$. The coefficients $F_{\mathbf{kk}'}$ and $K_{\mathbf{kk}'}$ will be discussed below.

We restrict attention to the two lowest degenerate modes with $\mathbf{k}_1 = (\pi/L, 2\pi/L)$ and $\mathbf{k}_2 = (2\pi/L, \pi/L)$ and their frequencies $\omega_{1,2} = (\pi/L)\sqrt{5T_0/\rho_0}$. We label these modes **1** and **2**. Quantizing, by imposing the commutation relation $[\hat{q}_{\mathbf{k}}, \hat{p}_{\mathbf{k}'}] = i\hbar\delta_{\mathbf{k},\mathbf{k}'}$, yields

$$H = \frac{\hat{p}_1^2 + \hat{p}_2^2}{2M} + \frac{M\omega_1^2}{2}\left(\hat{q}_1^2 + \hat{q}_2^2\right) + D\left(\hat{q}_1^4 + \hat{q}_2^4\right) + F\hat{q}_1^2\hat{q}_2^2 + K_1\hat{q}_1 + K_2\hat{q}_2 + K_{12}\hat{q}_1\hat{q}_2 + S_1\hat{q}_1^2 + S_2\hat{q}_2^2. \quad (4)$$

The terms in the first line of Eq. (4) are, respectively, the kinetic and potential energies of two harmonic oscillator modes. Due to the symmetry of the mode functions $\varphi_{\mathbf{k}}$, the quadruple sum in H_0 reduces to the two quartic terms in $\hat{H}$ with coefficients denoted by D and F. The terms in the second line of Eq. (4) originate from H_G, which is expanded to quadratic order. Compared to the fourth-order nonlinear Hamiltonian terms originating from the last term in H_0, the higher-order capacitive Hamiltonian terms are typically of the order of 10^{-6} and smaller and are negligible. The capacitive terms describe mode displacement, mode coupling, and harmonic frequency correction and are all voltage dependent. Introducing $\kappa \equiv \epsilon_0 L^2/u_0^2\pi^2$ the coefficients in Eq. (4) are

$$D \equiv \frac{161\pi^4 T_1}{4L^2}, \quad F \equiv \frac{41\pi^4 T_1}{2L^2}, \quad K_{1,2} = \kappa\left(V_1^2 \mp V_2^2\right),$$
$$K_{12} = -\frac{16\kappa}{9u_0}\left(V_1^2 - V_2^2\right), \quad S_{1,2} = -\kappa\pi^2 V_{1,2}^2/8u_0. \quad (5)$$

For time-dependent $V_{1,2}(t)$, the Hamiltonian Eq. (4) describes the excitation and evolution of two (nearly) degenerate interacting flexural modes. Also other modes, not included in Eq. (4), will be excited by the gates. This two-mode approximation is valid for weak intermode interaction and when the other modes are off resonance with the modes **1** and **2**.

For cat state generation we analyze the evolution of the system, initially in the ground state, subject to a common bias pulse on the two gates; i.e., $V_1 = V_2 = V_0\theta(t)$, where $\theta(t)$ is the unit step function. Then Eq. (4) reduces to

$$H = \hbar\sum_{j=1,2}\omega\left[\hat{a}_j^\dagger\hat{a}_j + \frac{\varepsilon}{4}(\hat{a}_j + \hat{a}_j^\dagger)^4\right] + \hbar\omega\delta(t)(\hat{a}_2 + \hat{a}_2^\dagger) + H_{12}, \quad (6)$$

where $\omega^2 \equiv \omega_{1,2}^2 + 2S_{1,2}/M$, $H_{12} = F\hat{q}_1^2\hat{q}_2^2$, $\varepsilon = D\hbar/M^2\omega^3$, and $\delta(t) = \sqrt{2}\kappa V_0^2\theta(t)/\sqrt{\hbar M\omega^3}$. The $\hat{a}_j^{(\dagger)}$ are defined through $\hat{p}_j = ip_0(\hat{a}_j^\dagger - \hat{a}_j)/\sqrt{2}$, and $\hat{q}_j = x_0(\hat{a}_j^\dagger + \hat{a}_j)/\sqrt{2}$ with $x_0 \equiv \sqrt{\hbar/M\omega}$ and $p_0 \equiv \sqrt{M\hbar\omega}$.

We consider the situation when the system is cooled to $k_B T \ll \hbar\omega$ and at time $t = 0$ the flexural modes are in their ground states $|0\rangle$. Equal voltage pulses are applied to both gates $\delta(t) = \delta_0\theta(t)$, inducing system's evolution. As mode **1** will not be appreciably affected by the weak coupling term H_{12}, the dynamics of the modes decouple. Hence, mode **1** will remain close to its ground state for $t > 0$. The remaining mode **2** describes a particle in a potential $v(\xi) = \sqrt{2}\delta_0\xi + \xi^2/2 + \varepsilon\xi^4$ with $\xi = q_2/x_0$ and an equilibrium position ξ_0. Introducing the displaced oscillator operator $b_2 = a_2 - \xi_0/\sqrt{2}$, and applying the rotating wave approximation (RWA), the Hamiltonian for mode **2** becomes $H_2 = \hbar\tilde{\omega}\hat{n}_b + 3\hbar\omega\varepsilon\hat{n}_b^2/2$, where

$$\hat{n}_b = \hat{b}_2^\dagger\hat{b}_2, \quad \tilde{\omega} = \omega\left[1 + 3\varepsilon\left(1/2 + 2\xi_0^2\right)\right]. \quad (7)$$

If $\varepsilon\xi_0^2 \ll 1$, the situation is similar to the one in Ref. 9. The intial state $|\psi(t=0)\rangle = |0\rangle_{a_2}$ resembles a coherent state in the b_2-basis, $|0\rangle_{a_2} \approx |-\xi_0/\sqrt{2}\rangle_{b_2}$. If the system evolves at time $t_1 = \pi/(3\omega\varepsilon)$, we expect to find the state

$$|\psi(t_1)\rangle \propto e^{-i\pi/4}|-\xi_0 e^{-i\tilde{\omega}t}/\sqrt{2}\rangle_{b_2} + e^{i\pi/4}|\xi_0 e^{-i\tilde{\omega}t}/\sqrt{2}\rangle_{b_2}, \quad (8)$$

which, to an overall phase, is in a basis given by

$$|\psi(t_1)\rangle \propto |\xi_0(1 - e^{-i\tilde{\omega}t})/\sqrt{2}\rangle_{a_2} + i|\xi_0(1 + e^{-i\tilde{\omega}t})/\sqrt{2}\rangle_{a_2}. \quad (9)$$

To verify this we simulated the dynamics using the full two-mode Hamiltonian in Eq. (4) and a Hilbert space of 40^2 number states in the occupation basis. The parameters used were $L = 126$ nm, $u_0 = 60$ nm, $T_0 = 0.003$ N/m, and $V_0 = 0.23$ V. This corresponds to $\omega/(2\pi) \approx 560$ MHz, $\varepsilon = 7 \times 10^{-4}$, and $\delta_0 = 1.3$. The position shift becomes $\xi_0 \approx -1.8 \approx -\sqrt{2}\delta_0$.

In Fig. 2(a), the probability density of finding mode **2** at a position ξ is shown as function of time. Only instants where $t = 2\pi n/\tilde{\omega}$ are sampled, hence, fast oscillations with frequency ω are not visible. The initial state $|0\rangle_{a_2} \approx |-\xi_0/\sqrt{2}\rangle_{b_2}$ evolves into a first catlike state at time $t_1 \approx 0.42\ \mu$s $\approx \pi/(3\omega\varepsilon)$. This and the following catlike state emerging at $t_2 \approx 1.27\ \mu$s $\approx \pi/(\omega\varepsilon)$ are marked with vertical dashed lines. The simulations also verified that mode **1** remains close to its ground state.

To read out the state, the two gates may form part of a capacitor in an LC-circuit with $\omega_{\mathrm{LC}} \gg \omega$ in the resolved sideband limit. This allows for side band cooling and measurement of

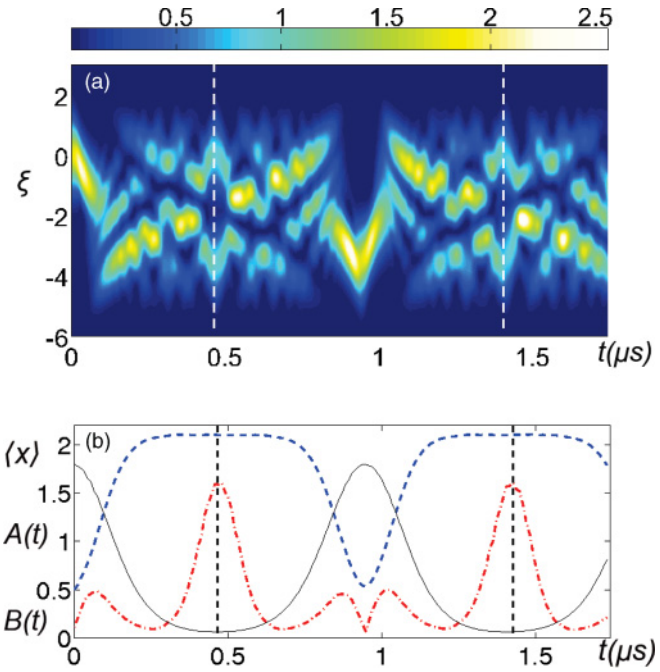

FIG. 2. (Color online) (a) False color plots of snapshots of time evolution of the position probability distribution for one flexural mode. The snapshots are taken at the turning points of the corresponding classical trajectory of the system. The positions (y axis) are scaled to the quantum zero point fluctuations x_0. (b) Corresponding time evolution of the envelopes of the quadrature $\langle X\rangle$ (continous line) and its associated quantum fluctuations $\langle \Delta X^2\rangle$; $A(t)$ (dashed line), $B(t)$ (dash-dotted line). The appearance of a cat state is signalled by a decrease in $\langle X\rangle$ along with an increased contribtion from quantum fluctuations $\langle \Delta X^2\rangle$ in the noise of $\langle X\rangle$. Vertical dashed lines indicate the agreement with (a).

the quadrature operator[21,22] $X_v = [e^{iv}a_2^\dagger + e^{-iv}a_2]/\sqrt{2}$. Using $v = 0$, this corresponds to a measurement of the position quadrature $\langle X\rangle$ and its quantum fluctuations $\langle \Delta X^2\rangle$, envelopes of which are shown in Fig. 2(b) as functions of time. The fluctuations have the form $\langle \Delta X^2\rangle \sim A(t) + B(t)\cos(2\omega t)$, where A and B evolve slowly in time. A signature of the built-up cat state is the reduction of $\langle X\rangle$ with an increase in $\langle \Delta X^2\rangle$. So far we have considered a closed system. A coupling to environment will, in general, cause damping and decoherence. For the cat state to emerge, dissipation must be weak. To estimate a lower bound on the resonator quality factor Q we note that even at zero temperature damping will cause decoherence. As shown in Refs. 13 and 14, for a linearly damped oscillator this occurs on a time scale $t_c \sim Q/\omega\xi_0^2$. Requiring $t_c \gg t_1$ yields $Q \gg \xi_0^2/\varepsilon$. For our protoype system, this inequality is fulfilled if $Q > 10^4$. Recently, Q factors up to $Q \sim 10^5$ were reported in graphene resonators.[18]

The cat state above is a product state between modes **1** and **2** in a basis. We now demonstrate a catlike state involving both modes that is not a product state in this basis. Preparing the system in the ground state $|0,0\rangle_a$ and switching on only one gate at time $t = 0$, i.e., $V_2 = 0$, $V_1 = \tilde{V}$, the degeneracy is lifted. Just as the operators $a_j^{(\dagger)}$ and $b_j^{(\dagger)}$, respectively, diagonalize the linear part of Eq. (4) when $V_{1,2} = 0$ and $V_1 = V_2 \neq 0$, the normal modes when $V_1 \neq V_2 = 0$ are found by diagonalizing the linear part of Eq. (4) by means of the transformation

$$\begin{aligned} d_1 &= \cos(\theta)a_1 - \sin(\theta)a_2, \\ d_2 &= \sin(\theta)a_1 + \cos(\theta)a_2 + \eta_0. \end{aligned} \tag{10}$$

Here $\eta_0 = \kappa\tilde{V}^2/\sqrt{\hbar M\omega^3}$ and we have neglected terms of order $|(\Omega_1 - \Omega_2)/\omega| \ll 1$, where $\Omega_{1,2}^2 = \omega^2 \mp K_{12}/M$ are the new eigenmode frequencies. The Hamiltonian Eq. (4) now transforms to

$$\tilde{H} = \hbar \sum_{j=1,2} \Omega_j d_j^\dagger d_j + \tilde{H}_{NL}, \tag{11}$$

where $\tilde{H}_{NL}$ is quartic in d operators. For degenerate modes the angle in Eq. (10) is $\theta = \pi/4$ and the nonlinear part in Eq. (11) becomes

$$\begin{aligned} \tilde{H}_{NL} = {} & \frac{\tilde{\varepsilon}}{4}(d_1 + d_1^\dagger)^4 + \frac{\tilde{\varepsilon}}{4}(d_2 + d_2^\dagger - 2\eta_0)^4 \\ & + \lambda(d_1 + d_1^\dagger)^2(d_2 + d_2^\dagger - 2\eta_0)^2, \\ \tilde{\varepsilon} = \hbar(2D - F)/4M^2\omega^3, & \quad \lambda = \hbar(6D - F)/2M^2\omega^3. \end{aligned} \tag{12}$$

As parameters like length and tension are never exactly equal in x and y directions, the two modes **1**,**2** are only approximately degenerate, $\omega_1 \neq \omega_2$. Hence, Eq. (12) is valid when the requirement $|(\Omega_1 - \Omega_2)/(\omega_1 - \omega_2)| \gg 1$ is fullfilled.

The initial state $|0,0\rangle_a$ is in d basis $|0,\eta_0\rangle_d$. After evolution with Eq. (11) this state will, analogous to the situation studied above, enter at time $\tilde{t}_1 \approx \pi/(3\omega\tilde{\varepsilon}) \approx 0.65\,\mu s$ the superposition

$$|\psi(\tilde{t}_1)\rangle \propto |0,\eta_0\rangle_d + i|0,-\eta_0\rangle_d + \alpha|\chi\rangle. \tag{13}$$

Here the last term $\alpha|\chi\rangle = \alpha\sum_{n=1}|n\rangle_{d_1}|\Psi_n\rangle_{d_2}$ is due to the quartic coupling term in Eq. (12). The state component $|0,\eta_0\rangle_d + i|0,-\eta_0\rangle_d$ corresponds to a catlike nonproduct state $|0,0\rangle_a + i|-\sqrt{2}\eta_0,-\sqrt{2}\eta_0\rangle_a$ in a basis.

To verify the creation of this state we numerically analyze the evolution of $|0,0\rangle_a$. Figure 3(a) shows the Wigner distribution $W(\xi_1,\pi_1) = (2\pi)^{-1}\int d\xi e^{-i\pi_1\xi}\langle\xi_1 + \xi/2|\hat{\rho}_1|\xi_1 - \xi/2\rangle$ of the reduced density matrix $\hat{\rho}_1$ of mode **1** in a basis at $\tilde{t}_1$. The distribution is plotted as function of the dimensionless position ξ_1 and momentum π_1 and has a bimodal structure. The distribution for mode **2** is identical, $W(\xi_2,\pi_2) = W(\xi_1,\pi_1)$.

To remove the remainder $\alpha|\chi\rangle$ from Eq. (13) we introduce the projection operators $\hat{P}_n = (|n\rangle\langle n|)_{d_1} \otimes \hat{I}_{d_2}$ and study [Fig. 3(b)] the Wigner distribution of the projection $\hat{P}_0|\psi(\tilde{t}_1)\rangle$. One can here clearly recognize the distribution corresponding to the state $|0,0\rangle_a + i|-\sqrt{2}\eta_0, -\sqrt{2}\eta_0\rangle_a$, which is displayed in Fig. 3(c) for reference. To ensure that the $\alpha|\chi\rangle$ component is of minor significance, the time evolution of the projections $\langle\hat{P}_0(t)\rangle$, $\langle\hat{P}_2(t)\rangle$, and $\langle\hat{I} - \hat{P}_0(t) - \hat{P}_2(t)\rangle$ are shown in Fig. 3(d).

The expression for $|\psi(\tilde{t}_1)\rangle$ in Eq. (13) is in RWA. In the Schrödinger picture the state has a fast oscillating component

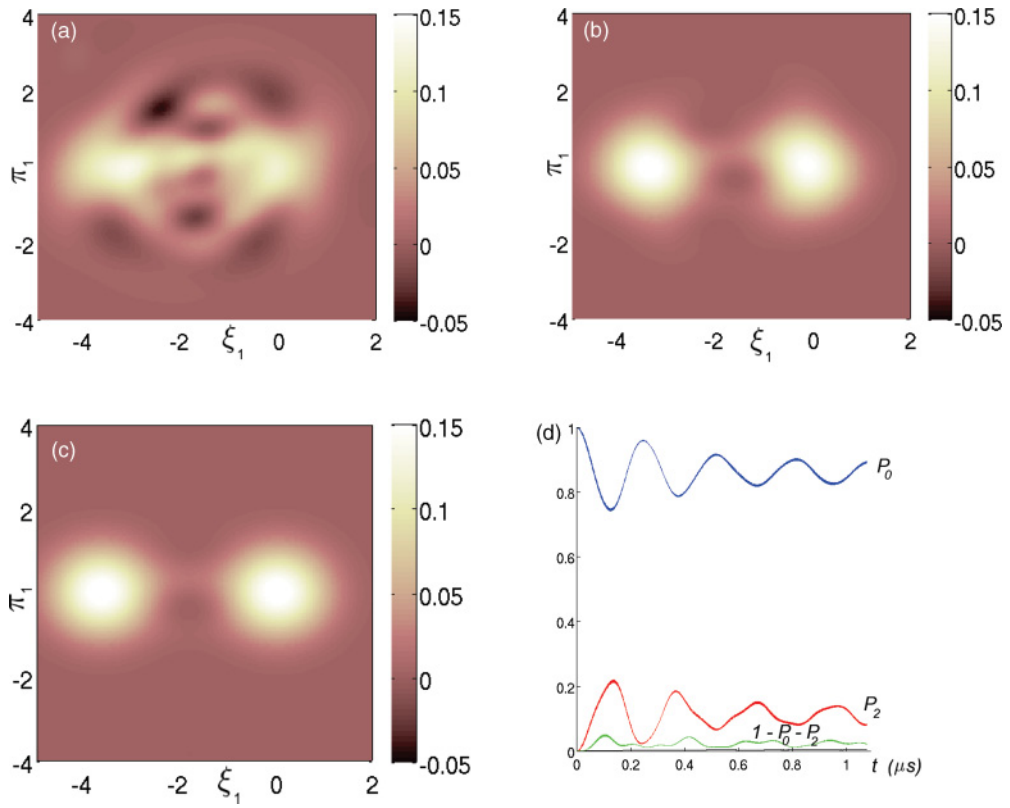

FIG. 3. (Color online) (a) False color plot of reduced Wigner distribution of the time evolved initial state $|0,0\rangle_a$, sampled at $\tilde{t}_1$ as function of the dimensionless position ξ_1 and momentum π_1. The Wigner distribution is obtained by numerically integrating the Hamiltonian Eq. (12). The reduced Wigner distributions are identical for both modes $W(\xi_1,\pi_1) = W(\xi_2,\pi_2)$. A bimodal structure is seen. (b) False color plot of Wigner distribution of $\hat{P}_0\hat{\rho}_1(\xi_1,\pi_1,\tilde{t}_1)\hat{P}_0$, clearly demonstrating bimodality. (c) False color plot of Wigner distribution of the analytic approximation $|0,0\rangle_a + i|-\sqrt{2}\eta_0,-\sqrt{2}\eta_0\rangle_a$. The similarity to the projection in (b) is evident. (d) Time evolution of projections $\langle\hat{P}_0(t)\rangle$, $\langle\hat{P}_2(t)\rangle$ and $\langle\hat{I} - \hat{P}_0(t) - \hat{P}_2(t)\rangle$. The most significant contribution is seen to come from $\langle\hat{P}_0(t)\rangle$.

and is at $t = \tilde{t}_1$ given by

$$\begin{aligned}|\psi(t)\rangle_S &= |0,\, \eta_0 e^{-i\tilde{\Omega}_2 t}\rangle_d + i|0,\, -\eta_0 e^{-i\tilde{\Omega}_2 t}\rangle_d + \alpha|\chi\rangle \\ &= \left|\frac{\eta_0}{\sqrt{2}}(e^{-i\tilde{\Omega}_2 t} - 1), \frac{\eta_0}{\sqrt{2}}(e^{-i\tilde{\Omega}_2 t} - 1)\right\rangle_a \\ &\quad + i\left|-\frac{\eta_0}{\sqrt{2}}(e^{-i\tilde{\Omega}_2 t}+1), -\frac{\eta_0}{\sqrt{2}}(e^{-i\tilde{\Omega}_2 t}+1)\right\rangle_a + \alpha|\chi\rangle.\end{aligned} \tag{14}$$

Here $\tilde{\Omega}_2$ is the eigenfrequency renormalized due to the nonlinearities in Eq. (12) [cf. Eq. (7)].

Similar behavior is seen for evolution from the initial state $|\eta_0,0\rangle_d = |0,\, -\sqrt{2}\eta_0\rangle_a$. Bimodality is then observable at $\tilde{t}_2 \approx 0.75\,\mu s$. We attribute the difference $\tilde{t}_2 - \tilde{t}_1$ to the position shift $2\eta_0$ in Eq. (12).

Finally, we demonstrate catlike nonproduct states in both a and d bases. Assume the cat state Eq. (9) was generated by the two-gate configuration at t_1. One gate is then switched off when $\tilde{\omega}t_1 = 2\pi m$, $m =$ integer. This kind of time-domain control has been shown possible in Ref. 23. The cat state is then a superposition of coherent states in d-basis $|\psi(t_1)\rangle \propto |0,\eta_0\rangle_d + i|-\xi_0,\xi_0 + \eta_0\rangle_d$. If $\tilde{V} = \sqrt{2}V_0$, then $\eta_0 \approx -\xi_0$, and the state is

$$|\psi(t_1)\rangle \approx |0,\eta_0\rangle_d + i|\eta_0,0\rangle_d. \tag{15}$$

As in previous cases, one would expect that after an evolution with Eq. (11) both modes would enter a superposition

$$|0,\eta_0\rangle_d + i|0,\, -\eta_0\rangle_d + i(|\eta_0,0\rangle_d + i|-\eta_0,0\rangle_d) + \beta|\zeta\rangle, \tag{16}$$

where $\beta|\zeta\rangle$ again is a small remainder due to the quartic coupling. Numerically we observe catlike states in both modes in time interval $0.72\ \mu s < \tilde{t}_1 < 0.82\ \mu s$. These are catlike superposition states, which are not product states in either a or d basis.

In analogy to the work of Yurke and Stoler,[9] we have shown that due to the intrinsic nonlinearities in graphene, generation of cat states and multimode cat states is possible by local back-gate manipulation. The nonlinearities are strong enough to avoid the necessity of coupling the membrane to an auxiliary system. In contrast to the system studied in Ref. 9, the nonlinearity and a weak intermode coupling are

always present in the graphene resonator, and an even stronger intermode coupling can be induced. Together with recent advancement in graphene device fabrication and improvement of cooling schemes this sets up further fundamental studies of macroscopic quantum phenomena.

The research leading to these results has received funding [A.V., A.I.] from the EU 7th framework programme (Grant No. FP7/2007-2013), QNEMS (Grant No. 233992), and the Swedish Research Council [J.M.K.]. We thank J. Atalaya and A. Croy for stimulating discussions.

*andreas.isacsson@chalmers.se

[1]C. Monroe, D. Meekhof, B. King, and D. Wineland, Science **272**, 1131 (1996).

[2]J. R. Friedman, V. Patel, W. Chen, S. K. Tolpygo, and J. E. Lukens, Nature (London) **406**, 43 (2000).

[3]S. Delglise, I. Dotsenko, C. Sayrin, J. Bernu, M. Brune, J. M. Raimond, and S. Haroche, Nature (London) **455**, 510 (2008).

[4]K. C. Schwab and M. L. Roukes, Phys. Today **58**, 36 (2005).

[5]A. D. O'Connell, M. Hofheinz, M. Ansmann, R. C. Bialczak, M. Lenander, E. Lucero, M. Neeley, D. Sank, H. Wang, M. Weides, J. Wenner, J. M. Martinis, and A. N. Cleland, Nature (London) **454**, 697 (2010).

[6]J. D. Teufel, T. Donner, D. Li, J. W. Harlow, M. S. Allmann, K. Cicak, A. J. Sirois, J. D. Whittaker, K. W. Lehnert, and R. W. Simmons, Nature (London) **475**, 359 (2011).

[7]M. Hofheinz, H. Wang, M. Ansmann, R. C. Bialczak, E. Lucero, M. Neeley, A. D. O'Connell, D. Sank, J. Wenner, J. M. Martinis, and A. N. Clealand, Nature (London) **459**, 546 (2009).

[8]C. W Gardiner and P. Zoller, *Quantum Noise* (Springer-Verlag, Berlin, 2000).

[9]B. Yurke and D. Stoler, Phys. Rev. Lett. **57**, 13 (1986).

[10]A. N. Cleland, *Foundations of Nanomechanics* (Springer, New York, 2003).

[11]I. Katz, R. Lifshitz, A. Retzker, and R. Straub, New J. Phys. **10**, 125023 (2008).

[12]M. I. Dykman, M. Marthaler, and V. Peano, Phys. Rev. A **83**, 052115 (2011).

[13]G. J. Milburn and C. A. Holmes, Phys. Rev. Lett. **56**, 2237 (1986).

[14]F. X. Kartner and A. Schenzle, Phys. Rev. A **48**, 1009 (1993).

[15]K. Jacobs, Phys. Rev. Lett. **99**, 117203 (2007).

[16]F. L. Semiao, K. Furuya, and G. J. Milburn, Phys. Rev. A **79**, 063811 (2009).

[17]J. Atalaya, A. Isacsson, and J. M. Kinaret, Nano Lett. **8**, 4196 (2008).

[18]A. Eichler, J. Moser, J. Chaste, M. Zdrojek, I. Wilson-Rae, and A. Bachtold, Nat. Nanotechn. **6**, 339 (2011).

[19]W. Soedel, *Vibrations of Shells and Plates* (Marcel Dekker, New York, 2004).

[20]K. N. Kudin, G. E. Scuseria, and B. I. Yakobson, Phys. Rev. B **64**, 235406 (2001).

[21]J. B. Hertzberg, T. Rocheleau, T. Ndukum, M. Savva, A. A. Clerk, and K. C. Schwab, Nat. Phys. **6**, 213 (2010).

[22]A. A. Clerk, M. H. Devoret, S. M. Girvin, F. Marquardt, and R. J. Schoelkopf, Rev. Mod. Phys. **82**, 1155 (2010).

[23]N. Liu, F. Giesen, M. Belov, J. Losby, J. Moroz, A. E. Fraser, G. McKinnon, T. J. Clement, V. Sauer, W. K. Hiebert, and M. R. Freeman, Nat. Nanotechnology **3**, 715 (2008).